Journal of Applied Mechanics and Technical Physics, Vol. 37, No. 4, 1996

BUBBLE CLUSTER, CUMULATIVE JETS, AND CAVITATION EROSION

V. K. Kedrinskii

UDC 532.528+620.193.16

Introduction. Experiments on laboratory modeling of ultrasonic cavitation erosion described in [1] show that a bubbly cluster develops in a liquid interlayer between the transformer and the tested sample in response to the action of tensile stresses in rarefaction phases. A frame of high-speed photographic record of the dynamics of the cavitation zone in Fig. 1 [1] shows a typical pattern of the process. The frequency of horn pulsations is 20 kHz, the amplitude is 3.9 μm, and the volume of the cavitation zone is 0.226 cm^3. It turned out that the bubbles in the zone pulsate almost in synchronism, and their frequency differs from the frequency of the external field produced by the horn.

Gas-vapor bubbles develop at so-called cavitation nuclei, i.e., heterogeneous inclusions which are almost always present in real liquids. The problems of their stabilization have not yet been completely solved. As an approach the Harvey model [2] is often used. It assumes the existence of cavitation nuclei as solid hydrophobic microparticles with slots inside which gas or vapor nuclei can be preserved.

Another type of structures, which are called combinative structures, was found experimentally by Besov et al. [3] who showed that microbubbles 1 could "attach" to the highly uneven surfaces of solid nuclei 2 (Fig. 2), thus ensuring stability of their suspension in a liquid. This structure also explains the effect of clarification of a liquid after passage of a shock wave as a result of destruction of the combinative structure and settling of solid nuclei free from gas bubbles.

Numerous studies (for example, [4–9]) confirm the importance of analysis of the individual interaction of a bubble with a solid surface whose damage is usually associated with the effect of shock waves and cumulative microjets that arise when the bubble collapses. The experimental data of [6–8] on correlation of the fine structure of the local damage zone with the hydrodynamic parameters of pulsation of an individual bubble in the cavitating liquid are of particular interest. These data indicated, in particular, the existence of a threshold energy barrier [7] and a monotone dependence of mass loss on the maximum bubble diameter $D_{\max}$, i.e., on the initial potential energy of the system $U_{\max}$ [8]. The energy is converted to the energy of a compression wave and the energy of a cumulative jet which arises during collapse of the bubble. It should be noted that, following [10], the amplitude of the shock wave generated by collapse of a single cavitation bubble is so small at the distance of the order of the initial-bubble radius that the shock wave cannot cause fracture of the sample.

The data of [8] were generalized in [11] as two relations for the mass loss per single load impulse:

$$\Delta g_1 \simeq 0.14\, U_{\max}, \qquad \Delta g_2 \simeq 3 \cdot 10^8 U_{\max}^3, \tag{1}$$

where Δg is measured in milligrams and $U_{\max}$ is measured in joules. The first relation is used for $U_{\max} \geqslant U_*$ and the second for $U_{\max} \leqslant U_*$, where $U_* \simeq 2.16 \cdot 10^{-5}$ J. Makarov et al. believe [8] that this relation determines the threshold of brittle fracture. The numerical coefficients and the value of $U_{\max}$ were obtained for aluminum.

As a rule, bubble cavitation is so intense that during its development the state of the medium and the parameters of the wave field are significantly changed. This naturally leads to the idea of representation

Lavrent'ev Institute of Hydrodynamics, Siberian Division, Russian Academy of Sciences, Novosibirsk 630090. Translated from Prikladnaya Mekhanika i Tekhnicheskaya Fizika, Vol. 37, No. 4, pp. 22–31, July–August, 1996. Original article submitted May 29, 1995.

 0021-8944/96/3704-0476 $15.00

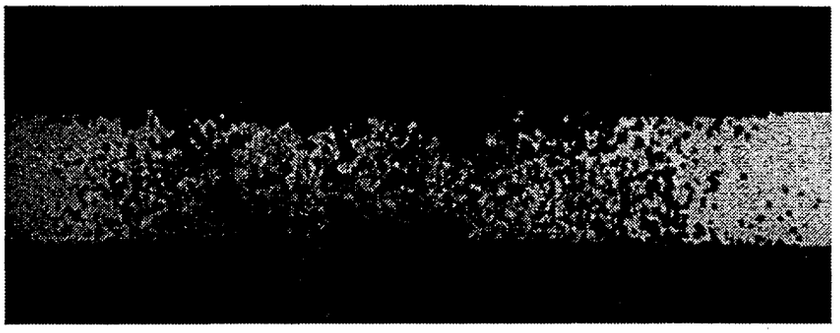

Fig. 1

of a real liquid as a two-phase medium. Applications of two-phase models to various formulations of erosion testing were first studied in [1, 12].

This approach is of importance, because, in spite of the local character of erosion effects, their frequency and intensity should depend on the hydrodynamic characteristics of the bubble cluster and the structure of the wave field in it. In this paper, we propose some approaches to the evaluation of erosion effects using a two-phase model of cavitating liquid and the generalization of experimental and numerical data on local damage of a sample by a cumulative microjet.

Single Cavity, Cumulative Jets (Experiment and Models). As was mentioned above, interesting experimental results for an incident-shock-wave–bubble–sample system were obtained by Sanada et al. [7], who studied for aluminum the dependences of the depth h_p of the cavity formed by an impact of a cumulative microjet on the amplitude p_{sh} of the shock wave which compresses the bubble near the sample and on the hardness H_V of the sample material. We use these results to determine the relation between jet penetration and the mass loss under a single load on the sample. It will be shown below that the frequency of action and its intensity can be determined only within the framework of a two-phase model of the dynamics of a cavitating liquid.

The cavity depth is $h_p \sim p_{sh}/H_V$ over a fairly wide range of parameters. It should be noted that in the classical problems of cumulative-jet penetration into targets the microhardness H_V enters the condition of equality of pressures at the jet–target interface and is considered a parameter responsible for dissipative processes:

$$\rho_j(V_j - V_p)^2/2 = \rho_m V_p^2/2 + H_V,$$

where V_p and V_j are the penetration velocity and the jet velocity, respectively. In particular, this condition makes it possible to determine the minimum velocity of a cumulative jet at which the jet does not penetrate into the target: $V_{j,\min} = \sqrt{2H_V/\rho_j}$. Thus, for values $H_V = 14$–70 MPa [7], the minimum velocity of the jet acting on the sample varies within 170–375 m/sec.

The experimental data of [7] show that for shock-wave amplitudes $p_{sh} \leqslant 35$ MPa an aluminum sample remains intact for any value of H_V within the above range: $h_p = 0$. It is obvious that for these values of p_{sh} and bubble radius $R_0 = 0.85$ mm the cumulative-microjet velocity does not exceed the strength threshold of the target. The above data may be interpreted as a threshold value of the initial potential energy of the system, which, in this case, is determined by the quantity $U_* \simeq 0.1$ J.

In the experiments of [7], the initial volume V_0 of the bubble was fixed; therefore, $h_p \sim p_{sh}V_0$ or $h_p \sim U_{\max}$, which is in agreement with data of [8]. Taking into account the character of flow transformation during cumulation it is reasonable to consider the dependence of h_p on $U_{\max}/S_j$, where $S_j = \pi d_j^2/4$ is the cross-sectional area of the jet. A new parameter appears which can be estimated as follows. Using the data of [7] we determine the pit diameter d_p as a function of the penetration depth h_p:

$$d_p \simeq 2h_p/(0.06 + 5.6 \cdot 10^{-3}h_p). \tag{2}$$

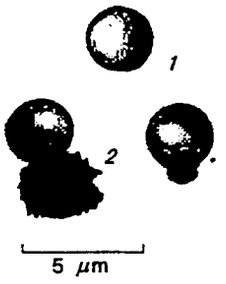

Fig. 2

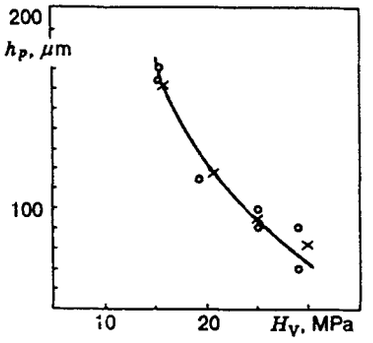

Fig. 3

The dimensions are given in micrometers. The relationship between d_j and d_p is estimated [13] within the framework of the classical cumulation theory for the one-dimensional problem of an infinite incompressible flow over a plate:

$$d_j/d_p \simeq 1 - 2\mu(1 + \tan\mu)/\pi,$$

where in terms of cumulation parameters $\tan\mu = V_p/(V_j - V_p) = \lambda$; $\lambda = \sqrt{\rho_j/\rho_m}$; and ρ_m is the density of the sample material (as is seen, for equal values of density, $V_p = V_j/2$). Substitution of the data on aluminum gives $d_j \simeq d_p/3$.

Finally, it is reasonable to assume that the jet diameter is proportional to the maximum bubble size R_* (or $y_* = R_*/R_0$). Then, the semi-empirical dependence of the penetration depth on the basic parameters of the problem and on the integral of the potential energy of the system is defined by

$$h_p \simeq 11.6\ R_0 \int_{y_{\min}}^{y_*} py^2 dy/H_V \tag{3}$$

(h_p and $\mathfrak{l}_0$, μm; p and H_V, MPa) The coefficient 11.6 is determined from the best data of [7].

For comparison the data calculated from relation (3) [7] are shown in Fig. 3 by crosses. The agreement is quite satisfactory. According to [13], when the target is made of soft materials, about 20% of the sample mass is ejected from the pit produced by a cumulative jet. If the pit is a cone, the ejected volume can be calculated from (2):

$$V_{\text{er}} \simeq h_p^3/(0.134 + 0.0125h_p)^2. \tag{4}$$

In (4) h_p is determined from (3). Under the assumption that precisely this mass governs the erosion effect (mass loss by the sample) for plastic materials, relation (1) allows one to estimate numerically the damage dynamics, if the density of the bubbles per unit area and their pulsation frequency are known. These parameters are found by analysis of the initial state of microinhomogeneities in the liquid and by solution of the problem of a cavitation cluster, respectively.

It should be noted that the above-mentioned threshold is not a single constraint in estimation of the erosion effect. The second basic constraint is the length of a cumulative jet. Following [14], the penetration depth L_p of a cumulative jet, the jet length L_j and density ρ_j, and the target-material density ρ_m, are related by $L_p = \lambda L_j$.

Thus, since a cumulative jet penetrates into a liquid only to the depth equal to its length ($\lambda = 1$), the presence of an interlayer between the cavitation bubble and the sample wall reduces considerably the effectiveness of jet action. As is clear from Kurbatskii's calculation of the axisymmetrical problem [15] of the

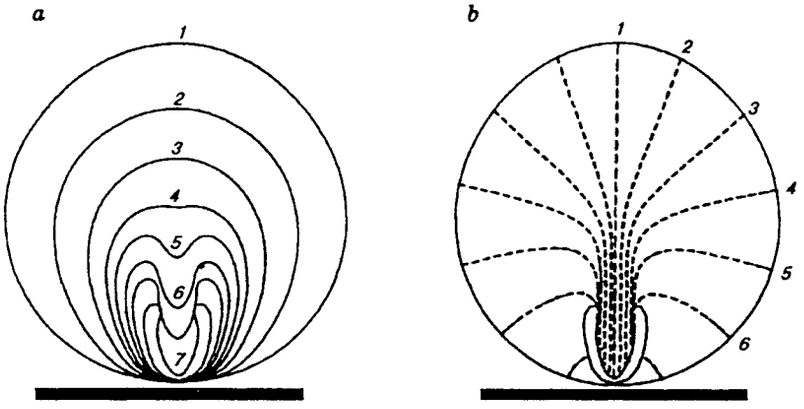

Fig. 4

collapse of an originally spherical hollow cavity near a solid wall, a microjet forms near the initial position of the center of the bubble even when the interlayer thickness is $L = 0.5R_{\max}$. The jet length is of the order of bubble half-radius ($L_j = L$) when the distance to the bubble is about three jet lengths. Although the velocity is fairly high (greater than 180 m/sec), such a jet cannot affect the sample.

When a bubble is in contact with a surface, a jet with length $L_j \simeq R_{\max}$ and diameter $d_j \simeq 0.2\ R_{\max}$ and with an almost uniform velocity field is generated. Figure 4 shows the dynamics of the bubble profile (a) and the particle trajectories 1–6 (b) for various times. Profile 2 corresponds to a dimensionless time of 0.8125, and profile 7 to 1.0906, and the time of collapse of a hollow cavity in an unbounded liquid is 1.0929 (1 is the initial profile). The velocity of the jet tip at the moment of contact with the lower boundary can be estimated as $V_j \simeq 1.3 \cdot 10^4 \sqrt{p/\rho_j}$, m/sec, if the pressure and density are measured in megapascals and kilograms per cubic meter, respectively. Thus, the above strength threshold for the contact of a bubble with a surface can be overcome for the softest material only when the external pressure p is not lower than 0.2 MPa. It can be shown that the kinetic energy of jets is only 0.4% of $U_{\max}$, which exceeds markedly the data of [8] (0.01%).

As to the external field, the above reasoning dealt with hydrostatics, and the bubble shape before callapse was arbitrary. Meanwhile, in practice, a cavitation bubble grows from a nucleus near the wall in the ultrasonic-field rarefaction phase. At the moment of maximum expansion the bubble takes the shape of an ellipsoid whose lower part is distorted versus the initial position of the nucleus. The bubble can move some distance away from the wall. Another feature of the real process is that the horn-induced external field is significantly distorted during the development of a cavitation zone because of energy consumption for its formation.

Bubble Cluster. As was mentioned above, erosion results from the collective action of a cavitation cluster. The dynamics of this action determines the characteristic collapse times, the dynamics of the pressure field in the cavitation zone, and the flow structure in the vicinity of an individual bubble near the solid wall. To make use of the above estimates, one should know how to calculate the above characteristics within the framework of a two-phase mathematical model.

Initial State of Liquid. Calculations of cavitation should be based on reliable data on the initial parameters of gas content: the volume concentration k_0 and the nucleus size R_0. To study the distribution of microinhomogeneities, we performed experiments with distilled water and fresh and settled tap water using the Malvern Instruments M 6.10 equipment with a magnetic mixer [11]. The measurements used the method of light diffraction by microinhomogeneities in liquids. The results are summarized in Tables 1 and 2, where t^* is the time of settling, k^* is the volume concentration of nuclei, R^* is the size of a nuclei, and β is the content of bubbles with radius R^* in the spectrum.

Table 1 presents data on the dynamics of gas content during settling of water, including the recorded

TABLE 1

Medium	t^*, h	k^*	R^*, μm
	0	$2.8 \cdot 10^{-4}$	40–120
Tap	2	$8 \cdot 10^{-6}$	1.2–15
water	17	$1 \cdot 10^{-6}$	1.2–10
	21	$< 1 \cdot 10^{-6}$	1.2–11
Distilled	0	$< 1 \cdot 10^{-6}$	1.2–13
water	24	$< 1 \cdot 10^{-6}$	1.2–3.4

TABLE 2

R, μm	β, %	
	Tap water	Distilled water
11.1	0.1	
9.6–8.3	10.7	
7.2–6.2	33.4	
5.3–4.6	31.1	
4–3.0	18.6	0.2
2.6	2.3	1.7
2.2	1.3	15
1.9	0.8	33.9
1.6	0.6	30
1.4	0.3	13.8

spectrum of nucleus radii R^*. The size distribution of cavitation nuclei for settling samples in percent is given in Table 2. One can see that the upper bound of the spectrum for tap water is considerably higher, and there are regions of intersection of the spectra. In distilled water, particles with size of 1.4–2.2 μm amount to more than 90% of the volume content of microinhomogeneities permitted by the method.

It should be noted that the resolution limit of the volume concentration for the equipment is 10^{-6}, and does not permit one to obtain quantitative data for the number of particles in the distribution, because it is difficult to select a standard test specimen. An estimate of the number of particles was obtained by analysis of the tracks of diffraction spots of microinhomogeneities which move in a laser beam because of natural heat convection.

The total number of microinhomogeneities of any nature in distilled-water sample reaches 10^5–10^6 cm^{-3}.

Two-Phase Model. Formulation of the Problem. We shall study the development of cavitation in thin liquid layers within the framework of a simple scheme which enables one to consider several variants of axisymmetric and plane formulations: an immovable rigid sphere with radius a is placed inside a hollow sphere (horn) with radius a_{ex} which is filled with water and oscillating with frequency f. The clearance δ between them is controlled by shifting their centers L.

Cavitating flow is described by the laws of conservation of mass and momentum for average characteristics and is closed by the relations between the mean density ρ, the volume concentration of the gas phase k, and the mean pressure p. The last two characteristics are related by the Rayleigh type equation for bubble concentration in a monodispere mixture. The governing system of equations describing the flow in a cavitating liquid is written as

$$\Delta p - c_0^{-2}\frac{\partial^2 p}{\partial t^2} = -\rho_0 k_0 \frac{\partial^2 k}{\partial t^2}; \tag{5}$$

$$\frac{\partial^2 k}{\partial t^2} = 3k^{1/3}(p_0 k^{-\gamma} - p)\rho_0^{-1} R_0^{-2} + \left(\frac{\partial k}{\partial t}\right)^2 (6k)^{-1}. \tag{6}$$

Here the subscript 0 refers to initial values; $k = (R/R_0)^3$; and R is the current radius of the cavitation bubble. This is a complete system for two basic characteristics of a cavitating medium (k, p). Under a series of assumptions Eq. (5) can be significantly simplified.

Ignoring the gas pressure in the bubbles and the inertial term in (6), which is justified for the rarefaction zone and acceptable for almost the entire range of bubble collapse, we obtain an approximate equation for the dynamics of the volume concentration:

$$\frac{\partial^2 k}{\partial t^2} \simeq -3k^{1/3} p \rho_0^{-1} R_0^{-2}.$$

Substituting it into (5) and assuming that the liquid component is incompressible, we obtain the equation

$$\Delta p \simeq (3k_0/R_0^2)k^{1/3}p. \tag{5'}$$

Let us introduce a new spatial variable $\eta = \zeta r$ ($\zeta = \alpha k^{1/6}$ and $\alpha = \sqrt{3k_0/R_0^2}$) assuming that $|p_{\eta\eta}\eta_r^2| \gg |p_r\eta_{rr}|$ and $k \gg |r\ k_r/6|$ (the subscripts denote the corresponding partial derivative, for example $p_{\eta\eta} = \partial^2 p/\partial\eta^2$); Eq. (5') can be reduced to the form [1, 16]

$$\Delta p \simeq p. \tag{7}$$

In our case of the axisymmetric problem of the development of cavitation in a narrow clearance between two spherical surfaces, the solution of (7) is represented as a combination of the Bessel functions $K_{n+1/2}(\zeta r)$ and the Legendre polynomials $P_n(\cos\theta)$ and becomes

$$p = \sum_n B_n r^{-1/2} K_{n+1/2}(\zeta r) P_n(\cos\theta). \tag{8}$$

We shall restrict ourselves to two terms of the series. Then, the approximate solution of (7) which determines the analytical dependence $p(k)$ is of the form

$$p \simeq \sqrt{\pi/2\zeta}\exp(-\zeta r) r^{-1}[B_0 + B_1(1 + 1/\zeta r)\cos\theta]. \tag{9}$$

The coefficients of Eq. (9) are found from the boundary conditions

$$\frac{\partial p}{\partial r} = 0 \quad \text{for} \quad r = a, \qquad \mathbf{n}\cdot\nabla p = -\rho_0\beta(t) \quad \text{for} \quad r = r_*.$$

Here $\mathbf{n}$ is a unit normal to the surface a_{ex}; $\beta(t) = -\mathbf{n}b\omega^2\sin(\omega t)$ is the acceleration of the surface, and b is the amplitude of the acceleration.

The pressure in the cavitating zone on the horn surface ($r = r^*$) is finally determined by the relation

$$p = p_0 + \rho_0 b r_* \omega^2 \sin(\omega t)[1 - (2 + \zeta a)r_*/(1 + \zeta a)a]/N, \tag{10}$$

where

$$N = \cos\gamma\{r_*(1 + \zeta r_*)[1 + (1 + \zeta a)^2]/a(1 + \zeta a) - [1 + (1 + \zeta r_*)^2]\} + \sin\gamma\tan\theta(1 + \zeta r_*);$$

$$\cos\gamma = (a_{ex}^2 - L^2 + r_*^2)/2r_* a_{ex}; \qquad r_* = \sqrt{a_{ex}^2 - L^2\sin^2\theta} - L\cos\theta.$$

The substitution of Eq. (10) into Eq. (6) reduces the problem to the solution of a second-order ordinary differential equation, in which the spatial coordinate r functions as a parameter. The angle θ is reckoned from the center line, the coordinate origin is placed at the center of the sphere a, and r_* is the coordinate of the point on a sphere with radius a_{ex}.

Analysis of the Calculation Results. According to the above data, the volume concentration k_0 was considered for values of 10^{-6}–10^{-12}. All calculations were performed for $R_0 = 1$ μm. Generally speaking, with allowance for the above experimental data on the spectrum of nuclei size system, (5) and (6) should be complicated: an individual equation of the type of Eq. (6) should be written for each part of the spectrum. However, as is shown in [12], an original polydisperse distribution structure rapidly becomes monodisperse in intense supersonic fields (Fig. 5). The calculation results for the expansion and collapse phases for bubbles (a) with various initial sizes (from 6 for R_1 to 2.88μm for R_{10}) obtained within the framework of a two-phase model and the pressure dynamics in the cavitating zone (b) are given in Fig. 5. The synchronous collapse of the bubbles indicates that the bubbles became equal in size, at least, at the moment the maximum size is reached.

In the present paper, we attempt to simulate the experimental result of [5] using the above estimates of erosion damage. In this case, our scheme of two spheres should have the following geometric parameters: $a_{ex} = 20$ cm, $a = 1$ cm, displacement of the centers $L = 18.95$ cm, and the clearance between the horn and the samples $\delta = 0.5$ mm. The frequency was 14.5 kHz.

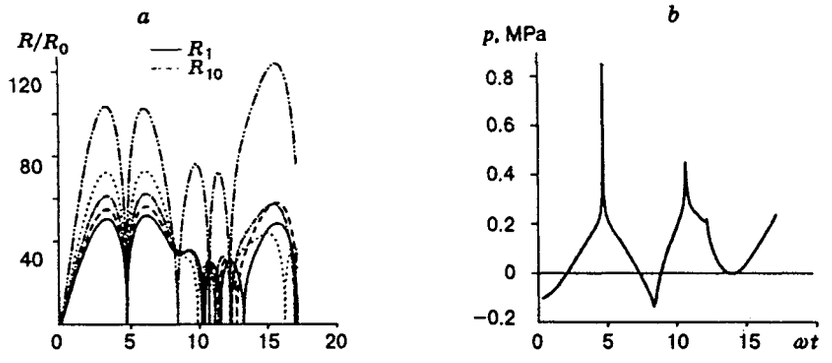

Fig. 5

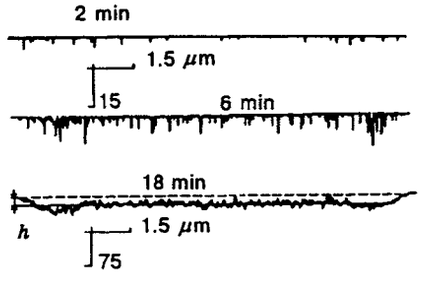

Fig. 6

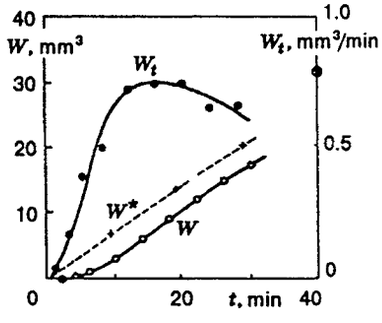

Fig. 7

A study of the fine structure of the pressure profile as a function of k_0 shows that an increase in its values from 0 or 10^{-12} to 10^{-6} with which the field amplitude decreases appreciably (although the wave profile remains unchanged) results in the gradual formation of the load pattern "permitted" by the cavitating liquid. In the cavitating liquid the vast majority of horn-induced waves is absorbed, and the loading rate increases appreciably. This gives rise to irregular peak loads with a fairly high amplitude in the clearance. The behavior and parameters of the cavitation bubble change abruptly as compared with its "single" dynamics [11].

Let us use the numerical interpretation (1) of the experimental data of [8] on the mass loss by the sample per single load impulse and try to relate the erosion rate to the potential energy of the bubble $U_{\max}$. It should be noted that these values are due to the fatigue effects occurring under long cyclical loading of the sample; therefore, the estimates for a single load may prove to be strongly averaged.

The potential energy $U_{\max}$ is determined by the integral $\int pdv$, and summation of it over all pulsations gives the dynamics of rates of the mass loss W_t^*. The calculation results for a vibration amplitude of $b = 25$ μm and a value of $k_0 = 10^{-8}$ averaged over the entire current time interval indicate that in the course of time the value W_t^* tends to stabilization at a level of about 0.1 mg/sec. Taking into account the closeness of the microhardness values of the samples $H_V = 140$ MPa [8] and $H_V = 133$ MPa [5], these calculations can be extended to the experiments of [5] with soft cermet materials with certain caution (the calculation is performed for tens of milliseconds but extended to minutes). From the function W_t one can easily estimate the dynamics of the mass loss $W(t)$, which, following [5], is close to the linear function $W \simeq 2(t-5)/3$ (t in minutes and W in cubic millimeters) over a time interval of 10–30 min.

Figure 6 shows a typical dynamics of the surface profile subjected to erosion for 2, 6, and 18 min with

various scales of vertical erosion depth [5]. The data on the dynamics of the volume loss $W(t)$ and the rate of losses W_t for the experiment are presented in Fig. 7. The dotted curves and crosses show the estimated values of $W^*(t)$. The estimate of the value W_t^* for $t = 40$ min obtained under the above assumptions is shown by an asterisk in a circle. Evidently, the order of the values is approximately the same.

The analysis performed shows that the two-phase model combined with approaches of the classical theory of cumulation allows estimation of erosion effects based on the extension of test results with accuracy to an order of magnitude, without considering the complete problem of the cavitation fracture of the samples. The calculation of the evolution of cavitation bubbles at microinhomogeneities [15] with allowance for the transformation of the pressure field in the cavitating liquid shows that there is an optimum position of the nuclei that determines, from the viewpoint of cavitation erosion, an optimal relation between the velocity and length of the cumulative jet and the distance to the wall.

REFERENCES

1. I. Hansson, V. Kedrinskii, and K. Morch, "On the dynamics of cavity clusters," *J. Phys., D, Appl. Phys.*, No. 15, 1725–1734 (1982).
2. E. N. Harvey, A. H. Whiteley, W. D. McElroy, et al., "Bubble formation in animals; II. Gas nuclei and their distribution in blood and tissues," *J. Cell. Compar. Physiol.*, **24**, No. 1 (1944).
3. A. S. Besov, V. K. Kedrinskii, Y. Matsumoto, et al., "Microinhomogeneity structures and hysteresis effects in cavitating liquid," Proc. 14th Int. Congress on Acoustics, Sept. 3–10, 1992, Beijing, China.
4. T. Okada, Y. Iwai, and A. Yamamoto, "A study of cavitation erosion of cast iron," *Wear*, No. 84 (1983).
5. T. Okada, Y. Iwai, and Y. Hosokawa, "Comparison of surface damage caused by sliding wear and cavitation erosion on mechanical face seal," *J. Tribol.*, No. 42 (1984).
6. Y. Tomita, A. Shima, and K. Takayama, "Formation and limitation of damage pits caused by bubble–shock wave interaction," in: *Proc. of National Symp. on Shock-Wave Phenomena*, Sagamihara, 1988. Tohoku Univ., Tohoku (1989), pp. 149–160.
7. N. Sanada, A. Asano, J. Ikeuchi, et al., "Interaction of a gas bubble with an underwater shock wave, pit formation on the metal surface," in: *Proc. of 16th Int. Symp. on Shock Tubes and Waves*, Aachen, 1987. VCH Publ., Weinheim (1988), pp. 311–317.
8. V. Makarov, A. A. Kortnev, S. G. Suprun, and G. I. Okolelov, "Cavitation erosion and spectrum analysis of pressure pulse heights produced by cavitation bubbles," in: *Nonlinear Acoustics*: Proc. of 6th Symp., Moscow State Univ., Moscow (1975), Vol. 2.
9. S. Fujikawa and T. Akamatsu, "Experimental investigations of cavitation bubble collapse by a water shock tube," *Bull. of ASME*, **21**, No. 152 (1978).
10. R. Ivany and F. Hammitt, "Cavitation bubble collapse in viscous compressible liquids: Numerical analysis," *Trans. of ASME, Ser. D*, No. 4 (1965).
11. V. K. Kedrinskii and V. A. Stepanov, "Cavitation effects in thin films," in: *Frontiers of Nonlinear Acoustics*: Proc. of 12th Int. Symp. on Nonlinear Acoustics, Austin, Texas, 1990. Elsevier Appl. Sci., London–New York (1990), pp. 470–475.
12. V. K. Kedrinskii, "Peculiarities of bubble spectrum behavior in cavitation zone and its effect on wave structure," in: *Ultrasonic Int. 85*: Proc. of Conf., London, Gilford (1985), pp. 225–230.
13. V. P. Alekseevskii, *To the Theory of the Armor-Piercing Action of a Shaped-Charge Jet* [in Russian], Kiev (1953).
14. M. A. Lavrentiev, "A shaped charge jet and its operation principles," *Usp. Mat. Nauk*, **12**, No. 4, 41–56 (1957).
15. K. A. Kurbatskii and V. K. Kedrinskii, "Collapse of a bubble in the cavitation zone near a rigid boundary," in: Abstr. of 124th Meeting of ASA, Oct. 31–Nov. 4, 1992. New Orleans (1992), pp. 2453.
16. V. K. Kedrinskii, "Propagation of perturbations in a liquid with gas bubbles," *Prikl. Mekh. Tekh. Fiz.*, No. 4, 29–34 (1968).